Micromechanical Mapping of Live Cells by Multiple-Particle-Tracking Microrheology

Yiider Tseng,*† Thomas P. Kole,* and Denis Wirtz*†‡
*Department of Chemical Engineering, †Graduate Program in Molecular Biophysics, and ‡Department of Materials Science and Engineering, The Johns Hopkins University, Baltimore, Maryland 21218 USA

ABSTRACT This paper introduces the method of live-cell multiple-particle-tracking microrheology (MPTM), which quantifies the local mechanical properties of living cells by monitoring the Brownian motion of individual microinjected fluorescent particles. Particle tracking of carboxylated microspheres imbedded in the cytoplasm produce spatial distributions of cytoplasmic compliances and frequency-dependent viscoelastic moduli. Swiss 3T3 fibroblasts are found to behave like a stiff elastic material when subjected to high rates of deformations and like a soft liquid at low rates of deformations. By analyzing the relative contributions of the subcellular compliances to the mean compliance, we find that the cytoplasm is much more mechanically heterogeneous than reconstituted actin filament networks. Carboxylated microspheres embedded in cytoplasm through endocytosis and amine-modified polystyrene microspheres, which are microinjected or endocytosed, often show directed motion and strong nonspecific interactions with cytoplasmic proteins, which prevents computation of local moduli from the microsphere displacements. Using MPTM, we investigate the mechanical function of α-actinin in non-muscle cells: α-actinin-microinjected cells are stiffer and yet mechanically more heterogeneous than control cells, in agreement with models of reconstituted cross-linked actin filament networks. MPTM is a new type of functional microscopy that can test the local, rate-dependent mechanical and ultrastructural properties of living cells.

INTRODUCTION

It is unclear whether and how the nonhomogeneous spatial distribution of cytoskeletal polymers such as F-actin, microtubules, and intermediate filament and their auxiliary proteins, leads to local variations of its mechanical properties. This is partly because in general there is no direct correspondence between the structure/organization and the mechanical behavior of a complex fluid. This is also because most current methods cannot readily measure the local mechanical properties of living cells (Tseng et al., 2002). Electron microscopy (EM) combined with immunocytochemistry and cryo-EM techniques have successfully been used to obtain detailed insight into the distribution and molecular interactions of macromolecular arrays in situ (Jarnik and Aebi, 1991; Schoenenberger et al., 1999; Penman, 1995). However, EM has not been extended to quantify the degree of spatial heterogeneity of networks, does not measure physical properties (e.g., cytoplasmic viscosity), and does not allow live-cell investigations. This last limitation can partially be alleviated by using correlative light and electron microscopy, which combines the live-cell capabilities of light microscopy and the superior spatial resolution of EM (Svitkina and Borisy, 1998). Confocal laser scanning microscopy can visualize the three-dimensional organization of cytoskeletal elements in situ (Vassy et al., 1997; Baschong et al., 1999) but makes use of fluorescent dyes that can affect intermolecular interactions and does not measure physical properties. Indeed, visualizing the actin cytoskeleton by fluorescence microscopy does not quantify its organization; e.g., enhanced fluorescence intensity of the F-actin may not necessarily mean enhanced heterogeneity. Magnetic tweezers were recently developed and used to probe the frequency-dependent viscoelastic moduli of living cells (Bausch et al., 1999; Wang and Ingber, 1995). However, large (magnetic) beads were used (1.3 μm) to reach a high enough probing force, and the specific/nonspecific interactions between the beads and subcellular structures were not characterized; moreover this approach is ill suited to probe the local subcellular response to an extracellular stimulus. By monitoring the diffusion of small, inert tracer particles via fluorescence microscopy, Ragsdale et al. (1997) probed the micromechanical properties of fibroblasts. However, many hypotheses were made to compute the cytoplasmic elasticity, and no global cellular response was obtained.

To monitor the local mechanical heterogeneity of cytoplasm and the viscoelastic response of living cells, we introduce a new functional microscopy, multiple-particle-tracking microrheology (MPTM) (Tseng et al., 2002). MPTM collects and analyzes the distribution of Brownian displacements of imbedded microspheres in the cytoplasm of live cells to spatially map its local viscoelastic properties. The approach can be intuitively understood as follows. The thermal energy k_BT creates a random force of order-of-magnitude k_BT/a on each microsphere, where

Submitted March 18, 2002, and accepted for publication September 30, 2002.

Y. Tseng and T. P. Kole contributed equally to this paper.

Address reprint requests to Dr. Denis Wirtz, Department of Chemical Engineering, Maryland Hall 221, The Johns Hopkins University, 3400 N. Charles St., Baltimore, MD 21218. Tel.: 410-516-7006; Fax: 410-516-5510; E-mail: wirtz@jhu.edu.

0006-3495/02/12/3162/15 $2.00

a is the radius of the microsphere. This minuscule force ($\ll$1 pN) creates a local dynamic deformation of the viscoelastic medium in the vicinity of the particle, which controls the particle's displacement, itself measured by video particle nano-tracking. By using a generalized Langevin equation of motion for a microsphere in a viscoelastic milieu (Xu et al., 1998a), mean squared displacement profiles are transformed into compliance profiles and viscoelastic parameters, which describe the local viscosity and elasticity of cytoplasm.

We illustrate the use of MPTM by investigating the changes in the mechanical properties of cytoplasm of Swiss 3T3 fibroblasts upon microinjection of purified α-actinin. α-Actinin is a ubiquitous actin cross-linking/bundling protein found in skeletal muscle, smooth muscle, and nonmuscle cells (Critchley, 1993). Rheological methods applied to in vitro models of actin filament networks containing purified actin and α-actinin, which in many ways mimic the somewhat heterogeneous actin cytoskeleton of non-muscle cells, suggest that α-actinin promotes the formation of stiff and viscous F-actin networks (Wachsstock et al., 1993). Quantitative ultrastructural studies of F-actin networks in vitro further predicts that α-actinin enhances the heterogeneity of the actin cytoskeleton (Tseng and Wirtz, 2001), but less so than fascin, another actin cross-linking/bundling protein (Yamashiro et al., 1998; Apgar et al., 2000). In contrast, the mechanical function of α-actinin's association with actin filaments in vivo has not been directly demonstrated. α-Actinin microinjected into cultured non-muscle cells localizes to stress fibers and focal adhesions (Izaguirre et al., 2001), which suggests that α-actinin stabilizes the actin cytoskeleton. The fact that α-actinin is expressed in concert with a multitude of other actin cross-linking proteins such as fascin greatly complicates the relatively simple picture provided by in vitro models of F-actin networks. Here, we test whether microinjected α-actinin enhances the elasticity, viscosity, and degree of heterogeneity of cytoskeleton in live cells in a manner similar to α-actinin-cross-linked actin gels in vitro.

In the first part of the paper, we describe MPTM, a new cell mechanics method that quantifies the local mechanical properties of live cells. By tracking the thermally excited displacements of fluorescent polystyrene (PS) particles embedded in the cytoplasm of Swiss 3T3 fibroblasts, distributions of mechanical compliance are generated and statistically analyzed. Analysis of the shape of the compliance distributions yields markers for the degree of mechanical heterogeneity of cytoplasm, which are compared with those obtained with reconstituted cytoskeletal networks. Particular attention is paid to the effects of particle surface charge and size on the apparent mean compliance and compliance distributions of the cytoplasm. In the second part of the paper, we use MPTM to investigate the mechanical function of α-actinin. We determine that microinjected α-actinin greatly increases cell strength but also enhances the degree of subcellular mechanical heterogeneity.

MATERIALS AND METHODS

Cell culture

Swiss 3T3 fibroblasts (American Type Culture Collection, Manassas, VA) were cultured at 37°C in 5% CO_2 in Dulbecco's modified Eagle's medium supplemented with 10% bovine calf serum (Life Technologies, Gaithersburg, MD). All measurements were performed at 37°C in 5% CO_2 in an incubator mounted on the inverted microscope used for the multiple-particle-tracking (MPT) measurements. Cells were grown on 35-mm glass-bottom dishes coated with poly-L-lysine (PLL; MatTek Corp., Ashland, MA).

Cytomechanics from multiple-particle tracking

To measure the local mechanical properties of cytoplasm, we modified the in vitro method of MPT introduced by Apgar et al. (2000). Yellow-green fluorescent PS microspheres (Molecular Probes, Eugene, OR) were microinjected into the cells and used as local probes of cytoplasm. The diameter of the microspheres was either 0.10 μm or 0.20 μm as specified. These microspheres were either carboxylated (negatively charged) or amine modified (positively charged) as specified. Cells microinjected with carboxylated or amine-modified microspheres were verified to continue to grow and divide normally more than 16 h after microinjection; moreover, cell morphology was unchanged compared with (neighboring) non-microinjected cells, and microspheres were passed to daughter cells. Cells microinjected with microspheres of different charge and size were examined in the same manner and within 10 min from each other as follows. Microspheres were microinjected following a modification of Beckerle's method (Beckerle, 1984) using the Eppendorf Transjector 5246 (Brinkmann Instruments, Westbury, NY). Fluorescent microspheres were extensively dialyzed against Dulbecco's PBS and subsequently diluted in Dulbecco's PBS to a final particle concentration of 10^{11} particles/ml solution. This solution was filtered through a 0.22-μm filter and stored at 4°C. The osmolarity of this solution was measured with a Wescor VAPRO vapor pressure osmometer (Wescor, Logan, UT) and found to be 285 mmol/kg, which is in the acceptable range for animal cells (Freshney, 1994). Borosilicate microneedles with a 0.3-μm inner diameter and 0.4-μm outer diameter (World Precision Instruments, Sarasota, FL) were back-loaded with 10 μl of the microsphere solution using micropipettes (Brinkmann Instruments). Cells within an area inscribed with a diamond-tipped pencil were microinjected at 37°C in a humidified, 5% CO_2 environment. After microinjection, cells were immediately washed with fresh media and incubated overnight in tissue culture medium.

The cells microinjected with the fluorescent particles were placed on the stage of a microscope at 37°C. Movies of the fluctuating fluorescent microspheres were recorded onto the (large) random-access memory of a PC computer via a silicon-intensifier target camera (VE-100 Dage-MTI, Michigan City, IN) mounted on an inverted epifluorescence microscope (Eclipse TE300, Nikon, Melville, NY) (Leduc et al., 1999). A $\times$100 Plan Fluor oil-immersion objective (N.A. 1.3) was used for particle tracking, which permitted an ~5-nm spatial resolution over a 120-μm $\times$ 120-μm field of view, as assessed by monitoring the apparent displacement of PS microspheres firmly attached to a glass coverslip with the same microscope and camera settings as used during the live-cell experiments. The thickness of the cell where microspheres are located is much larger than the diameter of the probe microspheres. Long-range interactions between the microspheres and the cell membrane could occur via hydrodynamic interactions, but those interactions are screened to within a mesh size of the cytoskeletal network, which is ~50 nm. The microspheres that we probe are not right at the cell edge; for instance, microspheres are rarely located within

filopodia. The microspheres were allowed to diffuse throughout the cells overnight. If the cell thickness were similar or smaller than the bead diameter, they would be mostly excluded from those (too thin) areas.

Movies of fluctuating microspheres were analyzed by a custom MPT routine incorporated into the software Metamorph (Universal Imaging Corp., West Chester, PA) as described (Tseng and Wirtz, 2001). The displacements of the particle centroids were simultaneously monitored in the focal plane of the microscope for 20 s at a rate of 30 frames per second. Between 12 and 42 particles per cell were tracked for a total of ~120 microspheres. These cells were chosen to have a similar shape and size as assessed by phase-contrast microscopy. Past that number of microspheres and number of cells, the shape of the mean squared displacement (MSD) distribution did not change with the number of probed microspheres and cells. Individual time-averaged MSDs, $\langle \Delta r^2(\tau) \rangle$, where τ is the time lag, were calculated from the two-dimensional trajectories of the centroids of the microspheres. We recently demonstrated that $\langle \Delta r^2(\tau) \rangle$ is proportional to the local compliance, $\Gamma(\tau) = (\pi a/k_B T)\langle \Delta r^2(\tau) \rangle$, of the specimen due to the small local force created by the fluctuating microsphere (Xu et al., 1998a). Here, k_B is Boltzmann's constant, T is the absolute temperature of the specimen, and a is the radius of the probe microsphere. From $\langle \Delta r^2(\tau) \rangle$ data, ensemble-averaged MSDs, $\langle\langle \Delta r^2(\tau) \rangle\rangle$, compliance values, $\Gamma(\tau)$, diffusion coefficients, $D(\tau)$, and MSD distributions were computed.

Viscoelastic moduli from particle tracking

All of the mechanical information is contained in the amplitude and the time-scale dependence of the compliance. However, for the sake of completeness, frequency-dependent elastic modulus $G'(\omega)$ and loss modulus $G''(\omega)$ were computed from time-lag-dependent MSDs as described (Mason et al., 1997b). Neglecting inertial effects, which become important only at microsecond time scales, and assuming that the fluid surrounding the probe particle is incompressible, the viscoelastic spectrum $G(s)$ is approximately given by:

$$G(s) = k_B T/\pi a s \langle \Delta r^2(s) \rangle$$

where s is the Laplace frequency, $\langle \Delta r^2(s) \rangle$ is the unilateral Laplace transform of $\langle \Delta r^2(\tau) \rangle$. This Laplace transform is computed over a limited range of time scales, which create errors as large as 12% (Mason et al., 1997b). The viscoelastic moduli $G'(\omega)$ and $G''(\omega)$ are the real and imaginary parts, respectively, of the complex modulus $G^*(\omega)$, which is the projection of $G(s)$ in Fourier space (Mason et al., 1997b). To illustrate the relation between $\langle \Delta r^2(\tau) \rangle$ and the local viscoelasticity, consider the displacements of a microsphere in a viscous liquid and in a Hookean solid, respectively. For a viscous liquid such as water or glycerol, the MSD of a microsphere of radius a in a liquid of viscosity η_0 is described by $\langle \Delta r^2(\tau) \rangle = 6D_0\tau$ (particle diffusion in three dimensions), where $D_0 = k_B T/6\pi\eta_0 a$ is the constant diffusion coefficient of the microsphere (Berg, 1993). Because $\langle \Delta r^2(s) \rangle = 6D_0/s^2$, we obtain $G(s) = \eta_0 s$ and the complex modulus is $G^*(\omega) = i\eta_0\omega$. Therefore, $G'(\omega) = \mathrm{Re}(G^*) = 0$ and $G''(\omega) = \mathrm{Im}(G^*) = \eta_0\omega$, as expected for a viscous, nonelastic liquid (Ferry, 1980). For a nondissipative Hookean solid of constant modulus G_0, the MSD of the same microsphere is independent of τ. Therefore, $\langle \Delta r^2(s) \rangle = A/s$ where $A = k_B T/\pi G_0 a$ is a constant, $G(s) = G_0$ and $G^*(\omega) = G_0$. Hence, $G'(\omega) = G_0$ and $G''(\omega) = 0$, as expected for a Hookean solid that exhibits negligible viscosity (Ferry, 1980).

Fluorescent labeling of actin cytoskeleton

Fluorescence microscopy was used to illustrate the heterogeneous organization of cytoskeletal actin in Swiss 3T3 cells. Cells were fixed in 3% paraformaldehyde in PBS (Life Technologies), made permeable with 0.1% Triton X-100 (Sigma, St. Louis, MO) in PBS, and labeled with rhodamine phalloidin (Molecular Probes). Fluorescently labeled cells were observed with a ×100, oil-immersion objective (N.A. 1.3) mounted on a Nikon Eclipse TE300 inverted microscope. Images were acquired with an Orca II CCD camera (Hammamatsu, Bridgewater, NJ) controlled by the Metamorph software. Specimens were mounted in Antifade (Molecular Probes) to minimize photobleaching.

Phase-contrast and differential interference contrast microscopy

The subcellular organization and morphology of live cells were revealed using either phase-contrast microscopy via a ×100 oil-immersion Plan Fluor lens (N.A. 1.3) or differential interference contrast (DIC) microscopy via a ×60 oil-immersion Plan Apo lens (N.A. 1.4; Nikon). These lenses were mounted on a Nikon Eclipse TE300 inverted microscope. Images were acquired with an Orca II CCD camera (Hammamatsu) controlled by the Metamorph software (Universal Imaging Corp).

Protein purification and microinjection

α-Actinin was purified from chicken smooth muscle as described (Xu et al., 2000). A 2-mg/ml α-actinin solution was injected into living cells 1 h before the MPTM measurements following published methods (Freshney, 1994). We estimate the final concentration of added α-actinin in the cells to be ~2 μM, which is smaller than the total concentration of endogenous α-actinin. Cells without added α-actinin, which serve as controls, were examined via MPTM, then microinjected with α-actinin, and reexamined 1 h after microinjection.

Nonspecific binding to microspheres

To asses the nonspecific binding of injected carboxylate- and amine-modified microspheres, we collected extracts of Swiss 3T3 cell lysates and incubated them for 24 h in the presence of the particles. The resulting suspensions were separated by centrifugation and analyzed by SDS-polyacrylamide gel electrophoresis and Pierce's bicinchoninic acid (BCA) protein assay kit. The BCA assay is used for the colorimetric detection and quantitation of total protein by monitoring the purple-colored reaction product of the well-known reduction product of Cu^{2+} to Cu^{1+} by protein in an alkaline medium (the Biuret reaction) using a unique reagent containing bicinchoninic acid (Pierce product 23225). A standard curve and equation for protein concentration versus absorbance was generated using the BCA kit on standard BSA samples of known concentration in concert with all unknown samples and plotting the measured absorbances at 562 nm against the known concentrations.

RESULTS

In this paper, we present a novel method, MPTM, to quantify the micromechanical properties and the intrinsic degree of mechanical heterogeneity of Swiss 3T3 fibroblasts. We then apply MPTM to test whether and how the F-actin cross-linking protein α-actinin affects the mechanical properties of cytoplasm.

MPTM of living cells

The spatial variation of the mechanical properties of the cytoplasm of Swiss 3T3 fibroblasts was assessed by statistically analyzing the distribution of displacements of microspheres imbedded in cytoplasm. Fluorescently labeled, 0.1-

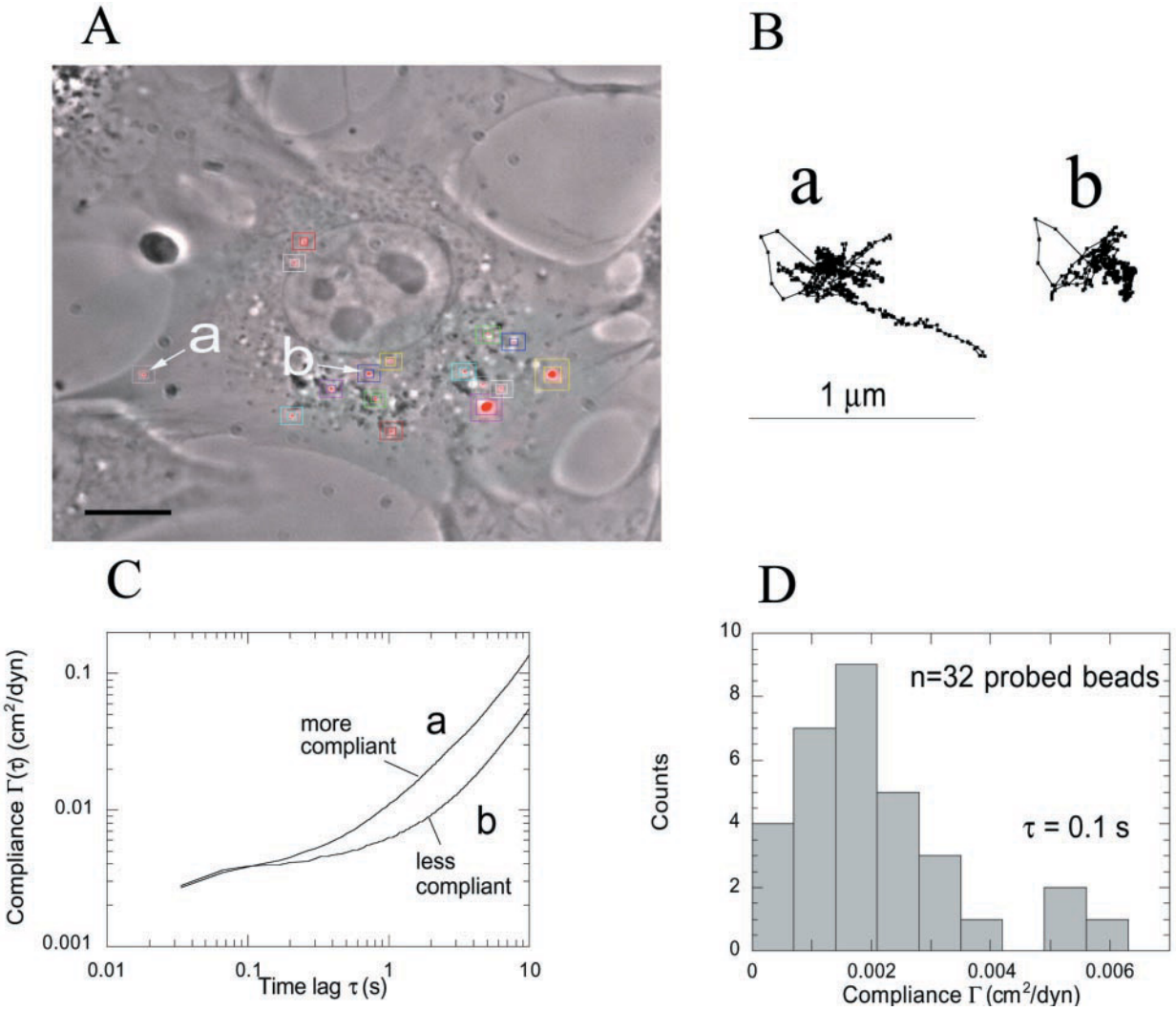

FIGURE 1 MPT of microspheres injected into live cells. The 0.1-μm-diameter, carboxylated PS microspheres were microinjected into Swiss 3T3 fibroblasts maintained in serum-containing medium and plated on a PLL glass microslide. The thermally excited motion of the particles was video tracked with 5-nm spatial resolution for 20 s. (*A*) Superposition of a phase-contrast micrograph with a fluorescence micrograph used for the identification and tracking of the probe microspheres. The inner boxes are drawn around the microspheres and help calculate the position of the microspheres' centroids. The outer boxes are the regions in which the tracking program checks for the position of the microsphere's centroid in the following frame. These positions of the boxes are updated in each new frame. The scale bar represents 20 μm. (*B*) Trajectories of microspheres *a* and *b*. These trajectories were verified to be uncorrelated by calculating their cross-correlation position function. (*C*) Local cytoplasmic compliance probed by the particles *a* and *b* shown in *B*. Creep compliance profiles are directly computed from individual MSDs. (*D*) Distribution of the local compliance of the cell shown in *A*. Compliance values were evaluated at a time scale of 0.1 s. The movements of 32 microspheres imbedded in the cytoplasm of the cell shown in *A* were analyzed.

μm-diameter carboxylated (negatively charged) PS microspheres were microinjected into 10 cells, which after a 12-h incubation, dispersed throughout the cytoplasm. We verified that the microinjection process did not affect normal cell growth and division in all tested conditions, and after division, daughter cells carried microspheres (data not shown). The centroids of the microspheres were monitored via time-resolved video light microscopy with ~5-nm spatial resolution and 33-ms temporal resolution (Fig. 1 *A*). Fig. 1 *B* shows examples of 20-s-long trajectories of microspheres localized to the lamella (*a*) and to the perinuclear region (*b*) of a Swiss 3T3 fibroblast. We note that the shape of a random walk is intrinsically anisotropic (Haber et al., 2000; Berg, 1993), and therefore, anisotropic features such as those displayed by the trajectory of particle *a* does not necessarily mean that nonstationary events (e.g., global cell motion and subcellular streaming) are occurring during particle tracking (see more below). We note that these cells were plated on PLL and can be considered immobile during each 20-s movie capture. From the time-dependent coordinates $[x(t), y(t)]$ of each microsphere, we computed the MSDs, $\langle \Delta r^2(\tau) \rangle = \langle [x(t + \tau) - x(t)]^2 + [y(t + \tau) - y(t)]^2 \rangle$, where t is the elapsed time and τ is the time lag or time scale (Tseng and Wirtz, 2001; Apgar et al., 2000). These MSDs

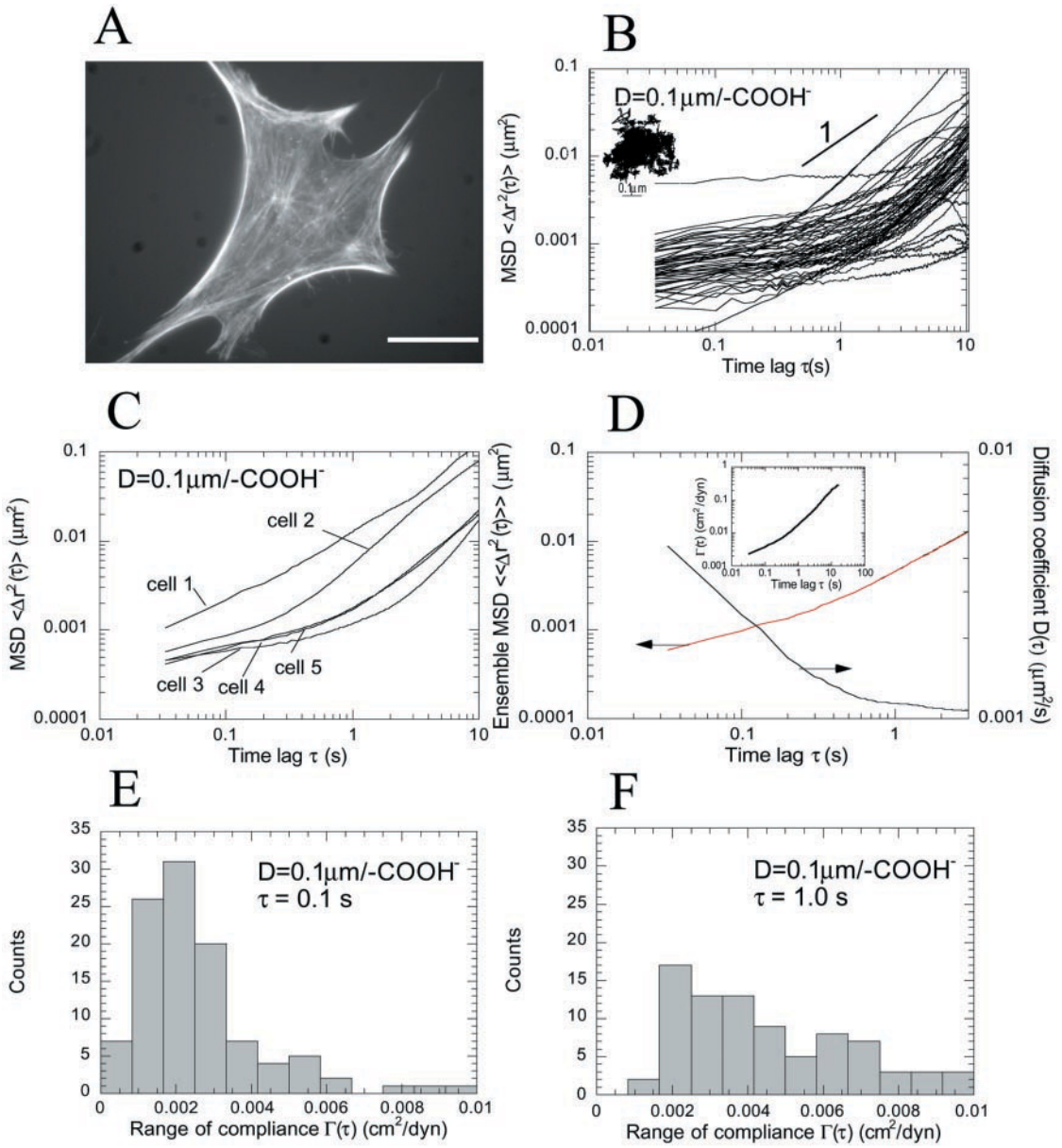

FIGURE 2 MPTM of living cells using 0.1-μm-diameter negatively charged microspheres. (*A*) Fluorescence micrograph of a Swiss 3T3 fibroblast fixed and stained for actin. The scale bar represents 30 μm. (*B*) Randomly selected MSDs of carboxylated microspheres injected into the cells 12 h before tracking. (*Inset*) Example of a trajectory of a microsphere's centroid, from which a MSD was calculated. (*C*) Cell-to cell variations of the mean MSD. The number of tracked particles per cell varied between 12 and 42. The average of the mean MSDs as well as the mean weighted by the number of particles per cell were nearly identical. (*D*) Diffusion coefficient (*right axis*) and ensemble-averaged MSD (*left axis*) after elimination of the directed contribution to the MSD (see Results for details). (*Inset*) Ensemble-averaged compliance of the cells: 1 $cm^2/dyn = 10\ Pa^{-1}$. (*E*) Distribution of subcellular compliance values measured at a time scale of 0.1 s. (*F*) Compliance distribution at a time scale of 1.0 s.

were transformed into time-scale-dependent compliance profiles, which describe the potential for cytoplasm to deform when subjected to the local force k_BT/a created by the thermal fluctuation of the probe microsphere. The time-lag-dependent compliance of the cytoplasm in the vicinity of the microspheres *a* and *b* are shown in Fig. 1 *C*, which illustrates the variations in the mechanical properties at different locations within the cytoplasm. The distribution of local compliance measured at a time scale of 0.1 s is shown for illustration in Fig. 1 *D*. This general approach, particle nanotracking and computation of the cytoplasmic compliance from the MSD, was automated to monitor and analyze the motion of ~120 microspheres per tested condition. We tested the effect of particle surface charge and size. These MSD profiles produced mean compliance values, compliance distributions, and distributions of local viscosity and elasticity.

Swiss 3T3 fibroblasts grown on PLL in the presence of serum displayed extensive F-actin bundles as detected by fluorescence microscopy (Fig. 2 *A*), which are distributed relatively heterogeneously throughout the cell (Hall, 1998). Using the methodology illustrated in Fig. 1, MSDs were collected in five cells and pooled (Fig. 2 *B*). At small time scales, most MSD profiles showed a quasi-plateau (defined here as a slower-than-linear increase of the MSD). This behavior is a hallmark of elastic trapping, whereby the microspheres are transiently prevented from readily diffusing through the cytoplasm due to the nonzero elasticity of their surrounding microenvironment. This effect is also observed when the same (negatively charged) microspheres are imbedded in reconstituted actin filament networks (Palmer et al., 1999) and intermediate filament networks in vitro (Ma et al., 2001). At intermediate time scales, the MSDs grew linearly with time (Fig. 2 *B*). This behavior, characterized by $\langle\Delta r^2(\tau)\rangle \sim \tau$, means that the interactions between the microspheres and their subcellular microenvironment are mostly viscous as in the classical Stokes-Einstein case. Finally, at long time scales ($\tau \approx 10$ s), MSDs grew slightly faster than time, a signature of activated transport, a behavior shown also by some outliers at earlier time scales (Fig. 2 *B*). The ensemble averaged MSD weighted by the number of microspheres per cell, $\langle\langle\Delta r^2(\tau)\rangle\rangle$, adopted a qualitatively similar profile (Fig. 2 *D*). This ensemble averaged MSD characterizes the global mechanical response of the cells and is used in our statistical analysis (see below). Mean MSDs were calculated for each cell in which the number of probe microspheres varied between 12 (cell 1) and 42 (cell 3) (Fig. 2 *C*). Cell-to-cell variations of the mean MSD were relatively large and may be due to the difference in the cell cycle coordination (Fig. 2 *C*). These results show that the cytoplasm of Swiss 3T3 fibroblasts plated on PLL in the presence of serum is mostly elastic at short time scales and viscous at long time scales. This means that these cells will elastically resist rapid shear deformations but not slow deformations.

The mean effective diffusion coefficient, $D(\tau)$, of the microspheres was directly computed from $\langle\langle\Delta r^2(\tau)\rangle\rangle$. The existence of nonstationary effects during particle tracking is readily detected by the shape of the MSD and is eliminated by curve fitting. To extract the mean diffusion constant D, in which we are primarily interested, and the mean directed velocity v of the microspheres, the polynomial $\langle\langle\Delta r^2(\tau)\rangle\rangle = 4D\tau + v^2\tau^2$ was fitted to the ensemble-averaged MSD $\langle\langle\Delta r^2(\tau)\rangle\rangle$ (Qian et al., 1991). This functional form contains both a random diffusion component, $4D\tau$, which dominates at short time scales, and a directed-transport contribution, $v^2\tau^2$, which dominates at long time scales. From the fit, we found an average velocity of $v \approx 6$ nm/s, which is much larger than the overall cell migration speed (data not shown). We note that, in contrast to conventional wisdom, the mean diffusion coefficient, $D(\tau) = \langle\langle\Delta r^2(\tau)\rangle\rangle/4\tau$ (having subtracted the directed transport component), was not constant and strongly decreased with time before reaching a plateau at long time scales (Fig. 2 *D*). This important result stems from the fact that $\langle\langle\Delta r^2(\tau)\rangle\rangle$ increased less slowly than linearly with τ. This τ-dependence, $\langle\langle\Delta r^2(\tau)\rangle\rangle \sim \tau^\alpha$ where $\alpha < 1$, describes a subdiffusive behavior (Chaikin and Lubensky, 1995; Saxton, 1994), which is presumably due to the elastic nature of the microfilament-rich microenvironment in the vicinity of the microspheres (Yamada et al., 2000).

The local compliance, $\Gamma(\tau)$, which describes the propensity of cytoplasm to locally deform (i.e., the inverse of stiffness), is directly proportional to the MSD (see Introduction). The ensemble-averaged compliance (total number of tracked particles was 114), $\langle\langle\,\Gamma(\tau)\rangle\rangle = (\pi a/k_BT)\langle\langle\Delta r^2(\tau)\rangle\rangle$ (corrected for directed transport as described above), which is the mean of all measured compliance profiles, showed a slow increase up to a time scale of $\tau \approx 0.3$ s (Fig. 2 *D inset*). This weak time dependence of $\Gamma(\tau)$ describes a viscoelastic microenvironment. Past $\tau \approx 0.3$ s, the compliance increased linearly with τ (Fig. 2 *D inset*), a signature of viscous behavior for which $\Gamma(\tau) = \tau/\eta$ where η is the viscosity (Ferry, 1980). The distribution of compliance values measured at a time scale of 0.1 s was wide (Fig. 2 *E*) and further widened at long time scales (Fig. 2 *F*). We shall show below how to rigorously analyze the shape of compliance distributions to quantify the degree of micromechanical heterogeneity of cytoplasm. But we first investigate the effect of particle surface charge and size on the apparent subcellular compliance.

Effect of particle surface charge and size

We probed the dependence of the apparent subcellular compliance and its distributions on particle size and surface charge. First, we compared the MSD profiles and compliance distributions obtained using 0.2-μm-diameter carboxylated microspheres with the measurements described above, which were obtained using 0.1-μm-diameter carboxylated microspheres. The MSD profiles of the larger particles (Fig. 3 *A*) were qualitatively similar to those obtained with the smaller particles (Fig. 2 *B*; compliance is proportional to MSD). Here again, most MSD profiles displayed a quasi-plateau at short times scales and a linear increase at long time scales. As expected, however, the amplitude of the MSD and associated diffusion coefficients (Fig. 4 *C*) of the larger particles were smaller than those of the smaller particles. The ensemble-averaged compliance profiles corresponding to the two radii overlapped over the entire tested time range, a result that is expected when the microspheres do not modify the local mechanical properties of the cell and do not directly interact with their surrounding microenvironment (see more in Discussion). Similarly to the 0.1-μm particles, cell-to-cell variations of the mean compliance measured by the 0.2-μm particles were relatively large (Fig. 4 *A*). Moreover, the distributions of compliance

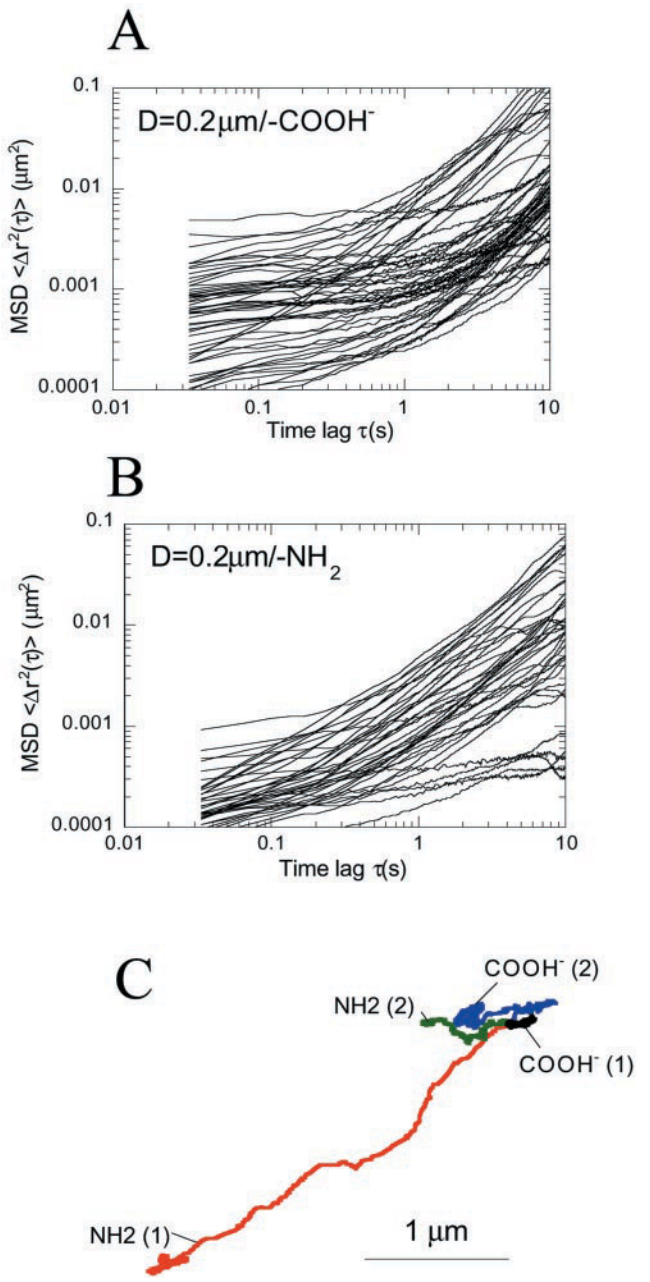

FIGURE 3 Measurements of the MSDs of 0.2-μm-diameter microspheres that are either positively or negatively charged. (*A*) Carboxylated (negatively charged) microspheres. (*B*) Amine-modified (positively charged) microspheres. (*C*) Typical trajectories of the centroids of amine-modified (denoted NH_2, green and red trajectories) microspheres and carboxylated microspheres (denoted $COOH^-$, blue and black trajectories).

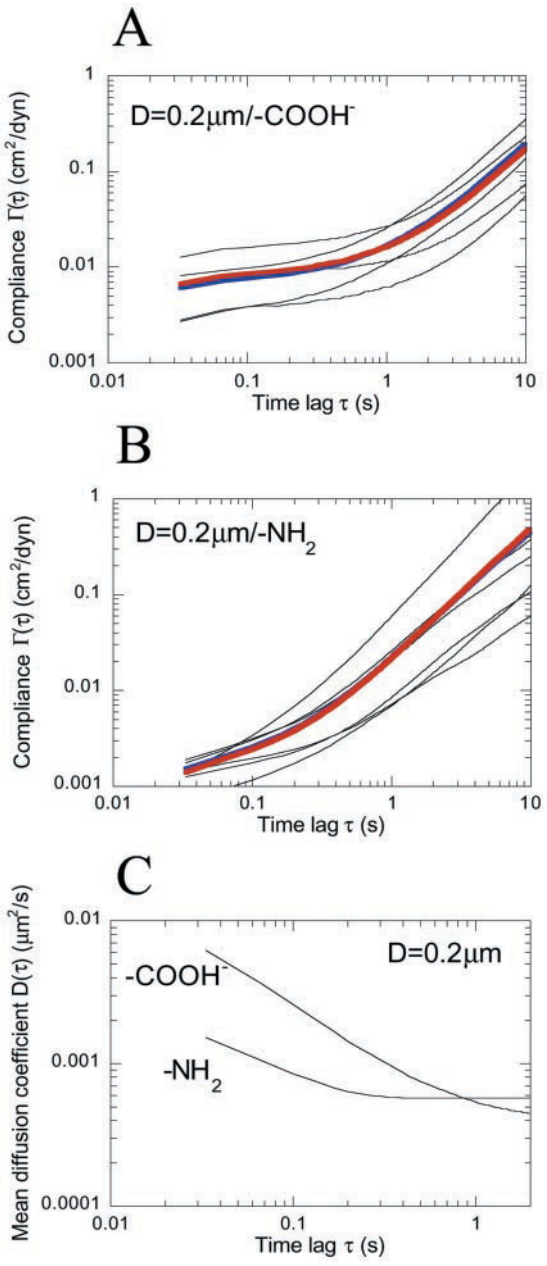

FIGURE 4 Mean cytoplasmic compliance and cell-to-cell variations of the compliance. (*A*) Carboxylated (negatively charged) microspheres. (*B*) Amine-modified (positively charged) microspheres. (*C*) Ensemble-averaged diffusion coefficients of carboxylated (denoted $COOH^-$) and amine-modified (denoted NH_2) microspheres. The directed-motion component was subtracted from the measured MSD to extract the random component of the MSD and the corresponding diffusion coefficient. Thin and thick lines represent individual-cell measurements and ensemble-averaged, respectively.

obtained with the 0.2-μm probes were similar to those obtained with the 0.1-μm probes (Fig. 5 *A* and Fig. 2, *E* and *F*). Finally, the shape of the compliance distributions was similar: the relative contributions of the highest compliance values to the mean cytoplasmic compliance for the 0.2-μm and 0.1-μm microspheres were nearly identical (Fig. 6; see more below). Amine-modified microspheres and carboxylated microspheres, which were embedded in cytoplasm via endocytosis, also displayed directed motion. Hence, endocytosis cannot be used to introduce beads to probe cell mechanics (data not shown).

To further asses the nonspecific binding of injected carboxylate- and amine-modified microspheres, we collected

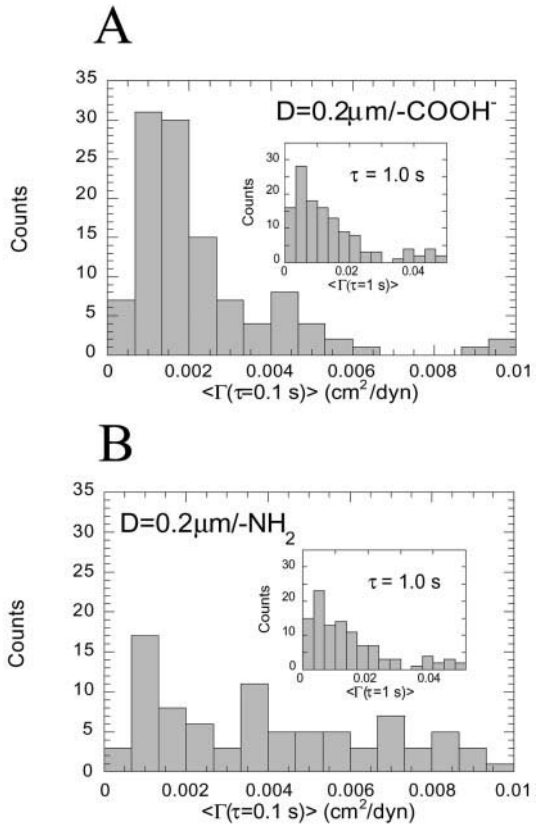

FIGURE 5 Distributions of the local compliance: effect of surface charge and size of the microspheres. (*A*) Distributions of the subcellular compliance measured at a time scale of 0.1 s using 0.2-μm-diameter carboxylated PS microspheres. (*Inset*) Compliance distribution at a time scale of 1.0 s. (*B*) Distributions of the subcellular compliance measured at a time scale of 0.1 s using 0.2-μm-diameter amine-modified PS microspheres. (*Inset*) Compliance distribution at a time scale of 1.0 s.

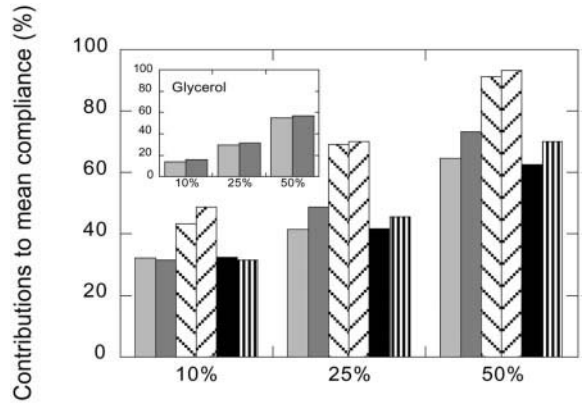

FIGURE 6 Statistical analysis of the compliance distributions. Contributions of the 10%, 25%, and 50% highest-compliance values to the mean creep compliance measured at different time scales. The first and second columns are for 0.1-μm carboxylated microspheres at time scales of 0.1 s and 1.0 s; the third and fourth columns are for 0.2-μm amine-modified microspheres at time scales of 0.1 s and 1.0 s; and the fifth and sixth columns are for 0.2-μm carboxylated microspheres at time scales of 0.1 s and 1.0 s.

cell lysate extracts and incubated them for 24 h in the presence of the particles. The resulting suspensions were separated by centrifugation and analyzed by SDS-polyacrylamide gel electrophoresis (not shown here) and the Pierce BCA protein assay kit. Using $\sim 3.6 \times 10^{13}$ particles per experiment, we found that in the presence of cell lysates, the carboxylate-modified particles bound $\sim 7.2 \times 10^{-14}$ μg of protein/particle whereas amine-modified particles bound $\sim 1.07 \times 10^{-12}$ μg of protein/particle. Considering actin as a model protein ($\sim$43 kDa), the mass of one actin molecule is 7.14×10^{-14} μg; thus, the carboxylate-modified particles bound only 1 actin molecule per microsphere, and the amine-modified microspheres each bound an average of 15 actin molecules.

The shape of the compliance profiles obtained using positively charged amine-modified microspheres was dramatically different both at short and long time scales from those observed with negatively charged particles. First, the extent of the displacements was much smaller at short time scales, which suggests the existence of strong interactions between the positively charged microspheres and their microenvironment (Figs. 3 *B* and 4 *B*). Second, at long time scales, the MSD rapidly grew faster than time, a strong evidence that amine-modified microspheres underwent saltatory directed motion (Figs. 3 *B* and 4 *B*). Indeed, positively charged particles often underwent bursts of directed, nonrandom motion through the cytoplasm (Fig. 3 *C*), possibly due to coupling of the microspheres to microtubule-based motor proteins. This type of large and rapid unidirectional intracellular movements were absent when negatively charged particles were used. Fitting of the apparent diffusion coefficient yielded directed (nonrandom) velocities that were on average $\sim$20 times higher than found with negatively charged particles. Due to this effect, the compliance distribution measured with positively charged, amine-modified particles was wide and skewed as measured by the bin distributions (Figs. 5 *B* and 6; see more below). These results suggest that a positively charged surface promotes nonrandom saltatory motion, which prevents the rigorous computation of the cytoplasmic compliance, at least at long time scales (see more in Discussion).

Degree of micromechanical heterogeneity

We observed relatively large cell-to-cell variations, but the shape of the compliance distribution did not vary when compliance values of more than four cells were pooled. To quantify the dispersion of the local compliance, we analyzed the compliance distribution in terms of bin distributions. The direct comparison of the shape of distributions that have different means may be somewhat misleading when one only considers absolute statistical parameters such as skewness and standard deviation. Therefore, we introduced

markers to quantify the relative degree of micromechanical heterogeneity of the cytoplasm of living cells: the relative contributions of the 10%, 25%, and 50% highest compliance values to the mean compliance (Fig. 6). These contributions should be exactly 10%, 25%, and 50% for a perfectly homogeneous liquid, which is what we observed when 0.1-μm-diameter, carboxylated PS microspheres were dispersed in a homogenous aqueous solutions of glycerol (Fig. 6 *inset*). These markers should become close to 100% in a highly heterogeneous milieu, which is observed, for instance, in a highly heterogeneous actin filament network in the presence of a high concentration of the F-actin cross-linking protein α-actinin (Tseng and Wirtz, 2001) and fascin (Apgar et al., 2000) and in concentrated DNA solutions (Goodman et al., 2002). Here, we found that the contributions of the 10%, 25%, and 50% highest-compliance values to the mean compliance of live cells were nearly identical when probed with particles of diameters 0.1 μm and 0.2 μm. This further suggests that carboxylated beads do not affect the mechanical properties and their distributions in live cells. These contributions were more than twice as high as measured in glycerol (Fig. 6 *inset*), which is expected given the heterogeneous nature of the actin cytoskeleton (Fig. 2 *A*), a major contributor to cell viscoelasticity (Yamada et al., 2000). These bin contributions were, however, much lower than observed with the positively charged probes (Fig. 6). Therefore, our results show that not only the amplitude of the mean compliance but also the relative distribution of compliance values did not vary with particle size for negatively charged microspheres.

Viscoelastic moduli of living cells

To further analyze the mechanical heterogeneity of cytoplasm, MSD traces were transformed into frequency-dependent viscoelastic moduli using Laplace transformation (Mason et al., 1997b; Xu et al., 1998a). The time lag dependence of the compliance of a viscoelastic fluid reflects the local viscoelastic properties of that fluid. $\Gamma(\tau) \sim \tau$ for a purely viscous liquid (e.g., water), $\Gamma(\tau)$ = constant for a purely elastic solid (e.g., steel), and $\Gamma(\tau) \sim \tau^{\alpha}$ with $0 < \alpha < 1$ for a viscoelastic material (e.g., F-actin networks (Palmer et al., 1999)). Here, each $\Gamma(\tau)$ trace was transformed into a frequency-dependent elastic modulus $G'(\omega)$ and viscous modulus $G''(\omega) = \eta(\omega)/\omega$ where $\eta(\omega)$ is the dynamic viscosity (see Materials and Methods). As expected from the compliance data, we found that elastic and viscous moduli were frequency dependent (Fig. 7) and displayed large local variations (bars in Fig. 7, *A* and *B*). For comparison, the viscosity of a glycerol standard (nominal viscosity 1 P), which is homogeneous, only varies between 0.92 and 1.08 P (Apgar et al., 2000); the elastic modulus of a 1-mg/ml F-actin solution varies between 15 and 25 dyn/cm^2 (at 1 rad/s) (Palmer et al., 1999). The cytoplasm behaved like a viscoelastic solid when subjected to high rates of deformations (second columns in Fig. 7, *A* and *B*). In contrast, as the compliance grew almost linearly with time at long time scales, the loss modulus became larger than the elastic modulus at low deformation frequencies. This means that the cytoplasm behaved like a viscoelastic liquid when subjected to low rates of deformations (first columns in Fig. 7, *A* and *B*).

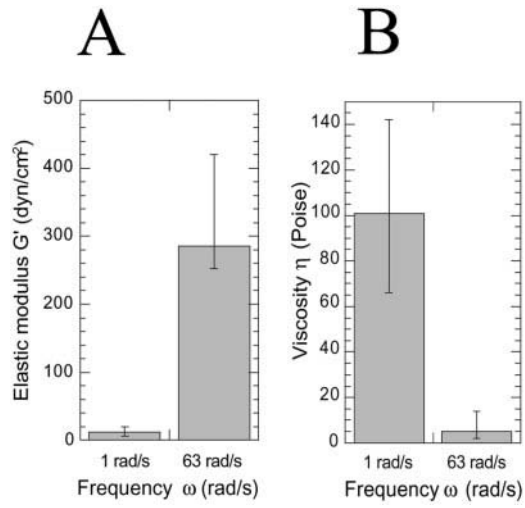

FIGURE 7 Viscoelastic moduli of living cells. (*A*) Elastic modulus of live cells at frequencies of ω = 1 rad/s and 63 rad/s; 1 dyn/cm^2 = 0.1 Pa. (*B*) Dynamic viscosity of live cells at frequencies of 1 rad/s and 63 rad/s; 1 Poise = 0.1 Pa s. The bars represent variations in moduli and viscosity. Elastic moduli and viscosities were computed from MSDs of microspheres imbedded within the cytoplasm via Laplace transformation as described in Materials and Methods and Results.

MPT mapping of the physical properties of cytoplasm

The physical properties of cytoplasm were mapped to specific regions within cytoplasm by combining MPTM and conventional DIC microscopy or phase-contrast microscopy. DIC microscopy shows the morphology of Swiss 3T3 fibroblast plated on PLL with superior contrast (Fig. 8); phase-contrast microscopy reveals the position of the microspheres with respect to intracellular organelles and nuclear/plasma membranes (Fig. 9, *A* and *B*). For each measurement, probe microspheres were microinjected 12 h before the MPT measurements, a time that allowed the microspheres to disperse throughout the cytoplasm (Figs. 8 and 9). To show variations in the physical properties of a single fibroblast plated on a PLL substratum, the measured compliance values were normalized by the maximum value and color-coded according to their amplitude between 0 and 1 (Fig. 9). Subcellular regions of small compliance (i.e., high stiffness) were color-coded blue, whereas regions of high compliance were color-coded red (Figs. 8 and 9 *A*).

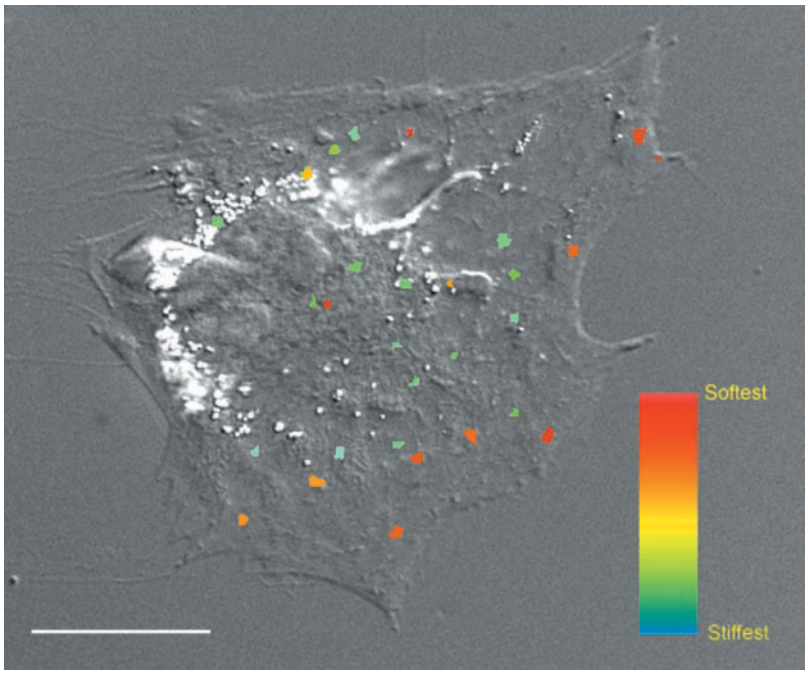

FIGURE 8 Multiple-particle microrheology mapping of a living cell. A DIC micrograph was superimposed to a fluorescence micrograph of the trajectories of microinjected microspheres. The trajectories, which were recorded for 20 s, were transformed into local compliances, which were normalized by the maximum compliance and color coded between red (most compliant microenvironment within the cell) to blue (least compliant microenvironment). Here, we used 0.1-μm-diameter carboxylated microspheres. Scale bar, 30 μm.

MPTM data can be further analyzed by computing the compliance as a function of the relative position ($0.0 < r_{rel} < 1.0$) of each particle with respect to the nuclear and cell membranes (Fig. 9 *B*). Here, $r_{rel} = 0.0$ denotes the nuclear membrane and $r_{rel} = 1.0$ denotes the plasma membrane as detected by phase-contrast microscopy. By using conventional phase-contrast and MPTM in concert, one can investigate the variations of the local compliance as a function of both time scale and the relative position of the microspheres in the subcellular region between the nuclear membrane and the cell surface (Fig. 9 *C*). By pooling compliance data of four randomly selected cells, we found that the perinuclear region, here defined as the subcellular region for which $0.0 < r_{rel} < 0.25$, was typically more compliant (i.e., less stiff) than the lamella, here defined as the subcellular region for which $0.25 < r_{rel} < 1.0$ (Fig. 9, *D* and *D′*).

α-Actinin enhances the stiffness and micromechanical heterogeneity of cytoplasm: a direct demonstration

Using MPTM, we can directly assess the effect of F-actin cross-linking proteins on the mechanical behavior of nonmuscle cells by adding exogenous α-actinin to cytoplasm. The F-actin cross-linking/bundling protein α-actinin is known to enhance the stiffness of F-actin networks in vitro (Xu et al., 1998b; Wachsstock et al., 1993; Grazi et al., 1993), a result that has not been directly tested in living cells. Here, we test this model of α-actinin-mediated stiffening in living cells by microinjecting purified α-actinin into control cells and subsequently using MPTM. Following the method presented in Figs. 1 and 2, we monitored the trajectories of a large number of 0.1-μm-diameter carboxylated PS microspheres and analyzed the time scale dependence and amplitude of the corresponding compliance profiles (Fig. 10 *A*). Mock injection of PBS led to no significant change in both the mean and distribution of MSDs, i.e., no change in the micromechanical properties of the cells (data not shown). The extent of the displacements of the probe microspheres imbedded in cells microinjected with α-actinin was typically significantly smaller than in control cells (Fig. 10 *A*). Globally, the time dependence of the compliance was slightly less pronounced than the controls (Fig. 10 *B*). The extent of the short-time-scale quasi-plateau of the average compliance was slightly enhanced, which suggests that filaments were (partially) prevented to move for longer time scales than in the control cells (Fig. 10, *A* and *B*). Cytoplasmic compliance was also greatly decreased; i.e., α-actinin induced a dramatic stiffening of cytoplasm, particularly at low rates of shear (Fig. 10, *A* and *B*).

Moreover, the distribution of compliance values in α-actinin-microinjected cells was much more skewed than in control cells. Bin-partition analysis indeed showed that the contributions of the 10%, 25%, and 50% highest-compliance values were significantly higher than those displayed by the control cells (Fig. 10 *C*). α-Actinin-injected cells

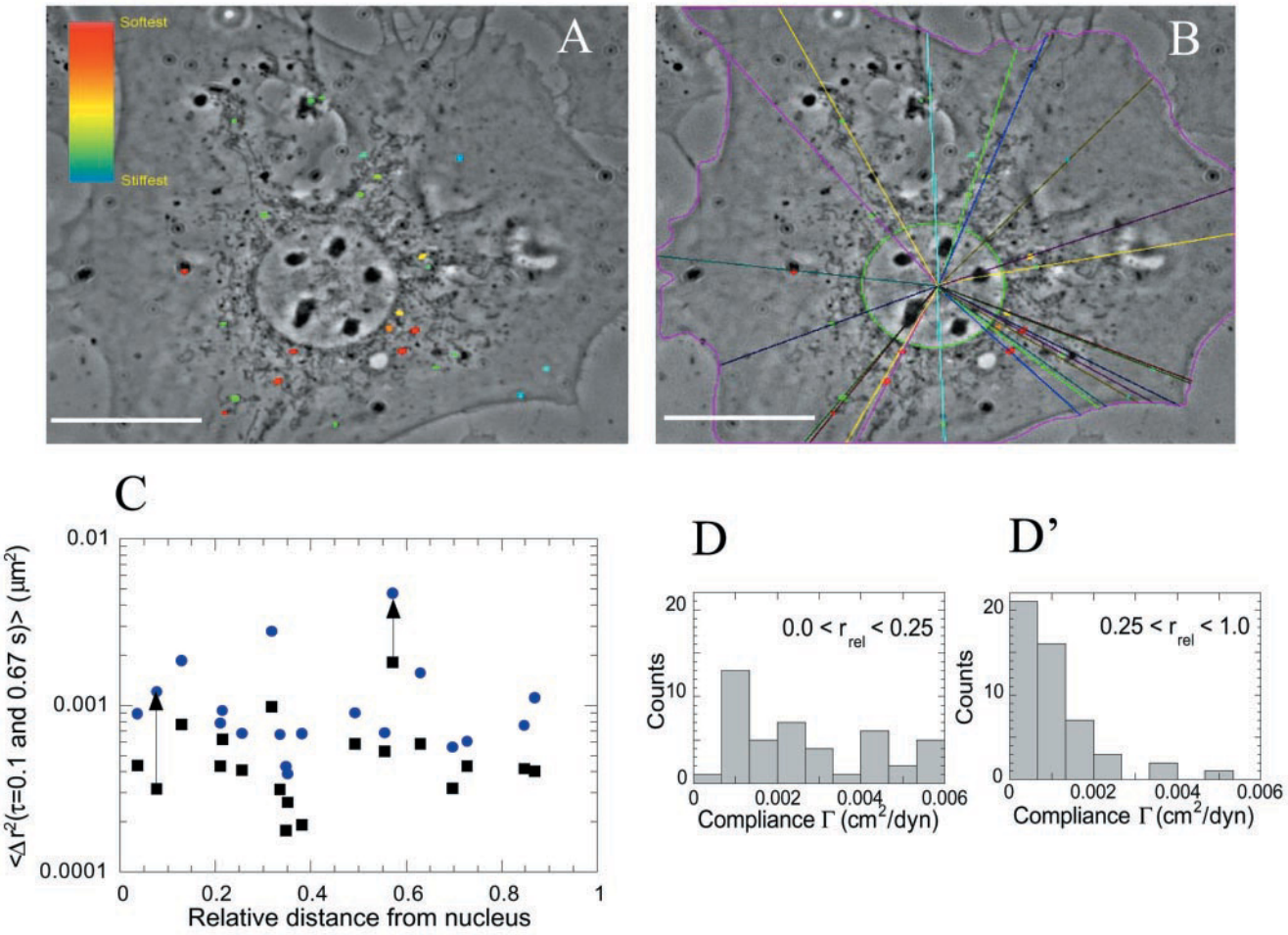

FIGURE 9 Subcellular compliance. (*A*) A phase-contrast micrograph was superimposed to a fluorescence micrograph of the trajectories of microinjected microspheres, which were color-coded according to the amplitude of their probed compliance at 20 s. Compliance values were normalized by the maximum. Scale bar represents 30 μm. (*B*) Plasma membrane and nuclear membrane were traced, and the relative position, r_{rel}, between 0 and 1, of each probe microsphere was computed. Scale bar represents 30 μm. (*B*) Obtained by phase-contrast microscopy. (*C*) Local compliance measured at time scales of 0.10 s (■) and 0.67 s (●). Arrows illustrate increases of compliance between 0.10 s and 0.67 s. (D and *D′*) Distributions of compliance values in the perinuclear region, defined here as the subcellular region for which $0.0 < r_{rel}, < 0.25$ and in the lamella defined as the subcellular region for which $0.25 < r_{rel}, < 1.0$.

displayed F-actin staining that was more intense but not obviously more heterogeneously distributed than in control cells (not shown).

DISCUSSION

MPTM, a new functional microscopy

We have introduced a new functional microscopy, MPTM, which probes the local micromechanics of living cells. To the best of our knowledge, no other approach delivers the instantaneous mapping of the local mechanical properties of a cell. Other cell-mechanics approaches either require detachment of the cell from its substrate (e.g., micropipette suctions), do not measure frequency-dependent moduli (e.g., AFM (Radmacher et al., 1994)), or do not probe local properties (e.g., magnetocytometry (Wang and Ingber, 1995)). MPTM measures not only the mean cytoplasmic stiffness but also its subcellular distribution. This approach is based on the statistical analysis of the MSDs of particles distributed throughout the cytoplasm. Because they constitute a relative marker, bin contributions of the compliance distributions can be compared directly with those obtained in reconstituted cytoskeletal networks or in other cells. MPT complements existing biophysical approaches, including light and electron microscopy, by quantifying the micromechanical heterogeneity in living cells. This paper focused on Swiss 3T3 fibroblasts and showed that the viscoelastic moduli of these cells depend on the frequency of the deformation. We further explored the capabilities of MPTM by mapping the micromechanical properties of the (soft) pe-

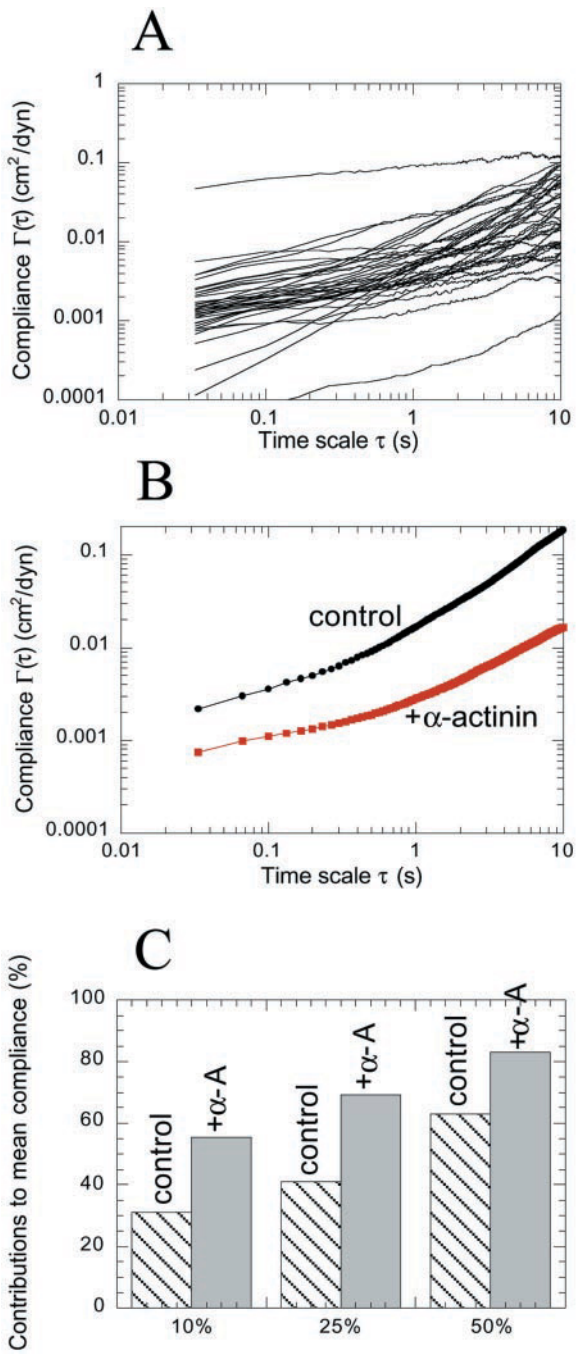

FIGURE 10 Micromechanics of α-actinin-microinjected cells. (*A*) Randomly selected compliance profiles in α-actinin-microinjected cells. (*B*) Ensemble-averaged compliance of α-actinin-microinjected cells and control cells. (*C*) Relative contributions of the 10%, 25%, and 50% highest-compliance values to the ensemble-averaged compliance. First columns correspond to control cells; second columns correspond to α-actinin-microinjected cells.

rinuclear region and the (stiffer) lamella of Swiss 3T3 fibroblasts. Finally, using MPTM, we demonstrated for the first time that the cross-linking protein α-actinin could stiffen the cytoskeleton and regulate its degree of heterogeneity in a manner identical to in vitro systems.

We found that the cytoplasm of fibroblasts behaves generally like a stiff elastic material when deformed rapidly and like a soft viscous liquid when deformed slowly. This behavior qualitatively matches the viscoelastic behavior of reconstituted actin filament networks in the presence of cross-linking proteins (Sato et al., 1987; Wachsstock et al., 1994; Bray and White, 1988; Xu et al., 2000). This viscoelastic behavior is particularly well suited to regulate cell migration (Bray, 2001). Activated processes, including the dendritic nucleation of actin at the leading edge and the contraction of the actomyosin machinery at the trailing edge of a motile cell, dominate the dynamics of cytoskeleton at the periphery. Those fast processes create large dynamic deformations of the cortical cytoskeleton, which generate membrane protrusions at the cell periphery and contractions at the trailing edge. Our results suggest that the cytoplasm will resist quick subcellular deformations such as those generated when the cell body, pushed and pulled by its dynamical periphery, crawls rapidly on its underlying substratum. Vice versa, the cytoplasm will soften in a slowly moving cell subjected to slow subcellular deformations, which in turn would enhance cell movement. This autoregulating mechanism for cell motion, the cytoplasm being stiff when the cell moves rapidly and soft when the cell moves slowly, consumes no energy because it is entirely passive.

We tested positively and negatively charged surfaces, using amine modification and carboxylation. In aqueous solutions, the carboxylate group displays a low nucleophilicity, and chemical groups that specifically react with carboxylic acids are rare. The carboxylated surface is also highly hydrophilic, which provides an ineffective surface for protein adsorption via hydrophobic interactions. Carboxylated microspheres have successfully been used to probe the local micromechanical properties of gels and networks. Quantitative agreement between particle tracking and diffusing wave spectroscopy microrheological methods using carboxylated microspheres and macrorheological measurements using a rheometer has been shown for a wide variety of complex fluids and cytoskeletal arrays in vitro. These include gliadin suspensions (Xu et al., 2002), concentrated DNA solutions (Mason et al., 1997a,b), aqueous solutions of polyethylene oxide (Mason et al., 1997b), poly(vinyl alcohol) aqueous solutions and chemically cross-linked gels (Narita et al., 2001), and actin filament networks over a large range of concentrations (Palmer et al., 1999). In contrast, many reactive groups are able to couple to amine-containing molecules. These reactions occur via acylation or alkylation and are often rapid, forming stable primary amide or secondary amine bonds (Hermanson, 1996). Our MPTM data at short time scales indeed suggest that the amine-modified microspheres used in our experiments are tightly bound to cytoplasmic structures, which artificially reduces the extent of the displacements at short time scales. Similar results were obtained with microspheres that were

deposited on the apical surface of cells and allowed to undergo endocytosis.

MPT offers numerous advantages over single-particle video and laser deflection tracking, recently introduced to probe the local viscoelastic properties of complex fluids (Mason et al., 1997b; Yamada et al., 2000; Gittes et al., 1997). Single-particle tracking, which measures local viscoelastic properties one particle at a time, is unsuitable to monitor fast spatiotemporal reorganization of the cytoskeleton, during, for instance, cell migration or cell division (Tseng et al., 2002). Figs. 8 and 9 show that MPTM is able to provide a global picture of the local stiffness of a single cell, a feat that cannot be achieved by single-particle tracking. Moreover, MPTM provides quantitative markers of the degree of mechanical heterogeneity of cytoplasm. Laser deflection particle tracking can probe only a very limited range of displacements, $\sim$0.4 μm (Mason et al., 1997b; Yamada et al., 2000), which prevents mechanical measurement at low frequencies (or long time scales), frequencies that are relevant to important cellular activities, including cell migration and cell spreading. Instead, MPTM probes more physiologically relevant (low) frequencies, over a large field of view, while preserving a superior spatial resolution.

The moduli of Swiss 3T3 fibroblasts measured here by MPTM were similar to those of COS7 cells measured by laser deflection single-particle tracking (Yamada et al., 2000). Moduli measured by AFM and the micropipette aspiration method tend to be higher, but these techniques may probe different mechanical properties (Hoh and Schoenenberger, 1994; Davies et al., 1997). Micropipette aspiration methods, in particular, measure the global properties of cells, mostly subjected to large deformations. AFM can probe the local elasticity of cytoplasm (Rotsch et al., 1997; Domke et al., 1999; Matzke et al., 2001) but does not measure the frequency response of the cell, and current rates of scanning prevent measurement of the global cellular response to rapid cellular activities.

Given the fact that the magnitude of moduli measured in Swiss 3T3 fibroblasts by MPTM and in COS7 cells by laser deflection particle tracking are similar, we focus our discussion on the degree of mechanical heterogeneity. We reanalyzed the compliance distributions obtained in COS7 using endogenous organelles as local viscoelastic markers (Yamada et al., 2000). We find that the contributions of the 10%, 25%, and 50% highest compliance values to the mean compliance is 31%, 42%, and 69% at a time scale of 0.1 s. These contributions are remarkably similar to those found in Swiss 3T3 fibroblasts grown in similar conditions, which further supports the use of exogenous carboxylated microspheres as markers of cytoplasmic viscoelasticity.

Besides probing the mechanical function of actin cross-linking proteins as shown in this paper, MPTM opens a realm of possibilities. Live-cell MPTM can be applied to quantify the degree of polarization of intracellular viscoelasticity in migrating cells subjected to chemoattractant gradients (Parent and Devreotes, 1999) or in the polarized cells of complex epithelia (Coulombe et al., 2000), two systems our group is currently investigating using MPTM. MPTM can be used to probe the micromechanical heterogeneity of cells subjected to extracellular factors (e.g., growth factors and lysophosphatidic acid) and various extracellular-matrix substrata (e.g., fibronectin and collagen), which cause cytoskeletal network reorganization by the activation of small GTPases (Burridge and Chrzanowska-Wodnicka, 1996). MPTM can also be used to monitor the spatiotemporal mechanical response of cells subjected to mechanical gradients of the substratum (Lo et al., 2000).

Mechanical function of α-actinin: a direct live-cell demonstration

The effect of α-actinin on F-actin network mechanics has been studied extensively in vitro. α-Actinin has been shown to enhance the elasticity of reconstituted F-actin networks (Wachsstock et al., 1993; Grazi et al., 1993) while increasing their degree of heterogeneity (Tseng et al., 2001; Tempel et al., 1996). To the best of our knowledge, however, no work has directly quantified the effect of α-actinin on the mechanical properties of live adherent cells. Here, using MPTM, we demonstrate that α-actinin can regulate the local and global mechanical behavior of fibroblasts. Exploiting the fact that MPTM provides local information, we find that the distribution of compliance in α-actinin-microinjected cells is significantly different from the control. Unlike MPTM, fluorescent staining of F-actin does not clearly determine that the increase in mechanical heterogeneity is due to α-actinin-mediated reorganization of the F-actin network. This shows that although fluorescence microscopy is very useful to document gross features of the cytoskeleton, it is unsuitable to quantify the cytoplasmic degree of mechanical heterogeneity. Our live-cell MPTM measurements corroborate previous rheological and particle-tracking measurements conducted in vitro, which show that α-actinin enhances the elasticity (Sato et al., 1987) and the degree of heterogeneity of reconstituted F-actin networks (Tseng et al., 2001). Our measurements also support previous demonstrations of the ϵ structural and mechanical functions of α-actinin (Pavalko and Burridge, 1991; Rivero et al., 1999). Our MPTM measurements in living cells therefore suggest that reconstituted networks constitute useful models of F-actin networks in non-muscle cells. Our results also suggest that different levels of expression of α-actinin would directly enhance the stiffness of cells and therefore affect their shape and propensity to deform during cell-migratory events. Following up on the present work, we recently found that an equimolar mixture of α-actinin and the actin cross-linking/bundling protein fascin synergistically produced F-actin structures that were significantly stiffer than

cells microinjected with α-actinin and fascin separately (Tseng et al., unpublished results).

We acknowledge financial support from the National Science Foundation (CTS0072278 and NIRT CTS0210718) and NASA through a graduate training grant (T.P.K.).

REFERENCES

Apgar, J., Y. Tseng, E. Federov, M. B. Herwig, S. C. Almo, and D. Wirtz. 2000. Multiple-particle tracking measurements of heterogeneities in solutions of actin filaments and actin bundles. *Biophys. J.* 79: 1095–1106.

Baschong, W., M. Duerrenberger, A. Mandinova, and R. Suetterlin. 1999. Three-dimensional visualization of cytoskeleton by confocal laser scanning microscopy. *Methods Enzymol.* 307:173–189.

Bausch, A. R., W. Môller, and E. Sackmann. 1999. Measurement of local viscoelasticity and forces in living cells by magnetic tweezers. *Biophys. J.* 76:573–579.

Beckerle, M. C. 1984. Fluorescent polystyrene beads exhibit saltatory motion in tissue-culture cells. *J. Cell Biol.* 98:2126–2132.

Berg, H. C. 1993. Random Walks in Biology. Princeton University Press, Princeton, NJ.

Bray, D. 2001. Cell Movements: From Molecules to Motility. Garland Publishing, New York.

Bray, D., and J. G. White. 1988. Cortical flow in animal cells. *Science.* 239:883–888.

Burridge, K., and M. Chrzanowska-Wodnicka. 1996. Focal adhesions, contractility, and signaling. *Annu. Rev. Cell. Dev. Biol.* 12:463–518.

Chaikin, P. M., and T. C. Lubensky. 1995. Principles of Condensed Matter Physics. Cambridge University Press, Cambridge, UK.

Coulombe, P. A., O. Bousquet, L. Ma, S. Yamada, and D. Wirtz. 2000. The 'ins' and 'outs' of intermediate filament organization. *Trends Cell Biol.* 10:420–428.

Critchley, D. R. 1993. Alpha-actinins. *In* Guidebook to the Cytoskeletal and Motor Proteins. T. Kreis and R. Vale, editors. Oxford University Press, Oxford, UK. 22–23.

Davies, P. F., K. A. Barbee, M. V. Volin, A. Robotewskyj, J. Chen, L. Joseph, M. L. Griem, M. N. Wernick, E. Jacobs, D. C. Polacek, N. dePaola, and A. I. Barakat. 1997. Spatial relationships in early signaling events of flow-mediated endothelial mechanotransduction. *Annu. Rev. Physiol.* 59:527–549.

Domke, J., W. J. Parak, M. George, H. E. Gaub, and M. Radmacher. 1999. Mapping the mechanical pulse of single cardiomyocytes with the atomic force microscope. *Eur. Biophys. J.* 28:179–186.

Ferry, J. D. 1980. Viscoelastic Properties of Polymers. John Wiley and Sons, New York.

Freshney, R. I. 1994. Culture of Animal Cells. John Wiley and Sons, New York.

Gittes, F., B. Schnurr, P. D. Olmsted, F. C. MacKintosh, and C. F. Schmidt. 1997. Microscopic viscoelasticity: shear moduli of soft materials determined from thermal fluctuations. *Phys. Rev. Lett.* 79:3286–3289.

Goodman, A., Y. Tseng, and D. Wirtz. 2002. Effect of length, topology, and concentration on the microviscosity and microheterogeneity of DNA solutions. *J. Mol. Biol.* 323:199–215.

Grazi, E., P. Cuneo, E. Magri, C. Schwienbacher, and G. Trombetta. 1993. Diffusion hindrance and geometry of filament crossings account for the complex interactions of F-actin with alpha-actinin from chicken gizzard. *Biochemistry.* 32:8896–8901.

Haber, C., S. Alom-Ruiz, and D. Wirtz. 2000. Shape anisotropy of a single random-walk polymer. *Proc. Natl. Acad. Sci. U.S.A.* 97:10792–10795.

Hall, A. 1998. Rho GTPases and the actin cytoskeleton. *Science.*279: 509–514.

Hermanson, G. T. 1996. Bioconjugate Techniques. Academic Press, San Diego, CA.

Hoh, J. H., and C. A. Schoenenberger. 1994. Surface morphology and mechanical properties of MDCK monolayers by atomic force microscopy. *J. Cell Sci.* 107:1105–1114.

Izaguirre, G., L. Aguirre, Y. P. Hu, H. Y. Lee, D. D. Schlaepfer, B. J. Aneskievich, and B. Haimovich. 2001. The cytoskeletal/non-muscle isoform of alpha-actinin is phosphorylated on its actin-binding domain by the focal adhesion kinase. *J. Biol. Chem.* 276:28676–28685.

Jarnik, M., and U. Aebi. 1991. Toward a more complete 3-D structure of the nuclear pore complex. *J. Struct. Biol.* 107:291–308.

Leduc, P., C. Haber, G. Bao, and D. Wirtz. 1999. Dynamics of individual flexible polymers in a shear flow. *Nature.* 399:564–566.

Lo, C. M., H. B. Wang, M. Dembo, and Y. L. Wang. 2000. Cell movement is guided by the rigidity of the substrate. *Biophys. J.* 79:144–152.

Ma, L., S. Yamada, D. Wirtz, and P. A. Coulombe. 2001. A hot-spot mutation alters the mechanical properties of keratin filament networks. *Nat. Cell Biol.* 3:503–506.

Mason, T. G., A. Dhople, and D. Wirtz. 1997a. Concentrated DNA rheology and microrheology. *In* Statistical Mechanics in Physics and Biology. D. Wirtz and T. C. Halsey, editors. 153–158.

Mason, T. G., K. Ganesan, J. V. van Zanten, D. Wirtz, and S. C. Kuo. 1997b. Particle-tracking microrheology of complex fluids. *Phys. Rev. Lett.* 79:3282–3285.

Matzke, R., K. Jacobson, and M. Radmacher. 2001. Direct, high-resolution measurement of furrow stiffening during division of adherent cells. *Nat. Cell Biol.* 3:607–610.

Narita, T., A. Knaebel, J. P. Munch, and S. J. Candau. 2001. Microrheology of poly(vinyl alcohol) aqueous solutions and chemically cross-linked gels. *Macromolecules.* 34:8224–8231.

Palmer, A., J. Xu, S. C. Kuo, and D. Wirtz. 1999. Diffusing wave spectroscopy microrheology of actin filament networks. *Biophys. J.* 76:1063–1071.

Parent, C. A., and P. N. Devreotes. 1999. A cell's sense of direction. *Science.* 284:765–770.

Pavalko, F. M., and K. Burridge. 1991. Disruption of the actin cytoskeleton after microinjection of proteolytic fragments of alpha-actinin. *J. Cell Biol.* 114:481–491.

Penman, S. 1995. Rethinking cell structure. *Proc. Natl. Acad. Sci. U.S.A.* 92:5251–5257.

Qian, H., M. P. Sheetz, and E. L. Elson. 1991. Single particle tracking: analysis of diffusion and flow in two-dimensional systems. *Biophys. J.* 60:910–921.

Radmacher, M., J. P. Cleveland, M. Fritz, H. G. Hansma, and P. K. Hansma. 1994. Mapping interaction forces with the atomic force microscope. *Biophys. J.* 66:2159–2165.

Ragsdale, G. K., J. Phelps, and K. Luby-Phelps. 1997. Viscoelastic response of fibroblasts to tension transmitted through adherens junctions. *Biophys. J.* 73:2798–2808.

Rivero, F., R. Furukawa, M. Fechheimer, and A. A. Noegel. 1999. Three actin cross-linking proteins, the 34 kDa actin-bundling protein, alpha-actinin and gelation factor (ABP-120), have both unique and redundant roles in the growth and development of *Dictyostelium*. *J. Cell Sci.* 112:2737–2751.

Rotsch, C., F. Braet, E. Wisse, and M. Radmacher. 1997. AFM imaging and elasticity measurements on living rat liver macrophages. *Cell. Biol. Int.* 21:685–696.

Sato, M., W. H. Schwarz, and T. D. Pollard. 1987. Dependence of the mechanical properties of actin/α-actinin gels on deformation rate. *Nature.* 325:828–830.

Saxton, M. J. 1994. Anomalous diffusion due to obstacles: a Monte Carlo study. *Biophys. J.* 66:394–401.

Schoenenberger, C. A., M. O. Steinmetz, D. Stoffler, A. Mandinova, and U. Aebi. 1999. Structure, assembly, and dynamics of actin filaments in situ and in vitro. *Microsc. Res. Tech.* 47:38–50.

Svitkina, T. M., and G. G. Borisy. 1998. Correlative light and electron microscopy of the cytoskeleton of cultured cells. *Methods Enzymol.* 298:570–592.

Tempel, M., G. Isenberg, and E. Sackmann. 1996. Temperature-induced sol-gel transition and microgel formation in α-actinin cross-linked actin networks: a rheological study. *Phys. Rev. E.* 54:1802–1808.

Tseng, Y., E. Fedorov, J. M. McCaffery, S. C. Almo, and D. Wirtz. 2001. Micromechanics and microstructure of actin filament networks in the presence of the actin-bundling protein human fascin: a comparison with α-actinin. *J. Mol. Biol.* 310:351–366.

Tseng, Y., T. P. Kole, S.-H. J. Lee, and D. Wirtz. 2002. Local dynamics and viscoelastic properties of cell biological systems. *Curr. Opin. Colloid. Int. Sci.* 7:210–217.

Tseng, Y., and D. Wirtz. 2001. Mechanics and multiple-particle tracking microhetrogeneity of alpha-actinin-cross-linked actin filament networks. *Biophys. J.* 81:1643–1656.

Vassy, J., T. Irinopoulou, M. Beil, and J. P. Rigaut. 1997. Spatial distribution of cytoskeleton intermediate filaments during fetal rat hepatocyte differentiation. *Microsc. Res. Tech.* 39:436–443.

Wachsstock, D., W. H. Schwarz, and T. D. Pollard. 1993. Affinity of α-actinin for actin determines the structure and mechanical properties of actin filament gels. *Biophys. J.* 65:205–214.

Wachsstock, D., W. H. Schwarz, and T. D. Pollard. 1994. Crosslinker dynamics determine the mechanical properties of actin gels. *Biophys. J.* 66:801–809.

Wang, N., and D. E. Ingber. 1995. Probing transmembrane mechanical coupling and cytomechanics using magnetic twisting cytometry. *Biochem. Cell Biol.* 73:327–335.

Xu, J., Y. Tseng, C. J. Carriere, and D. Wirtz. 2002. Microrheology and microheterogeneity of wheat gliadin suspensions studied by multiple particle tracking. *Biomacromolecules.* 3:92–99.

Xu, J., Y. Tseng, and D. Wirtz. 2000. Strain-hardening of actin filament networks: regulation by the dynamic crosslinking protein α-actinin. *J. Biol. Chem.* 275:35886–35892.

Xu, J., V. Viasnoff, and D. Wirtz. 1998a. Compliance of actin filament networks measured by particle-tracking microrheology and diffusing wave spectroscopy. *Rheol. Acta.* 37:387–398.

Xu, J., D. Wirtz, and T. D. Pollard. 1998b. Dynamic cross-linking by α-actinin determines the mechanical properties of actin filament networks. *J. Biol. Chem.* 273:9570–9576.

Yamada, S., D. Wirtz, and S. C. Kuo. 2000. Mechanics of living cells measured by laser tracking microrheology. *Biophys. J.* 78:1736–1747.

Yamashiro, S., Y. Yamakita, S. Ono, and F. Matsumura. 1998. Fascin, an actin-bundling protein, induces membrane protrusions and increases cell motility of epithelial cells. *Mol. Biol. Cell.* 9:993–1006.